The American Journal of Pathology, Vol. 171, No. 6, December 2007

DOI: 10.2353/ajpath.2007.061144

Tumorigenesis and Neoplastic Progression

Nox1 Expression Determines Cellular Reactive Oxygen and Modulates c-fos-Induced Growth Factor, Interleukin-8, and Cav-1

Rebecca S. Arnold,*† Ju He,* Andrea Remo,*‡ Darren Ritsick,‡ Qiqin Yin-Goen,‡§ J. David Lambeth,‡ Milton W. Datta,*‡ Andrew N. Young,‡§ and John A. Petros*†‡§

From the Departments of Urology, Pathology,‡ and Laboratory Medicine,† Winship Cancer Institute, Emory University School of Medicine, Atlanta; and the Atlanta Veterans Administration Medical Center,§ Decatur, Georgia*

Increased cellular reactive oxygen species (ROS) can act as mitogenic signals in addition to damaging DNA and oxidizing lipids and proteins, implicating ROS in cancer development and progression. To analyze the effects of Nox1 expression and its relation to cellular ROS and signal transduction involved in cellular proliferation, Nox1RNAi constructs were transfected into DU145 prostate cancer cells overexpressing Nox1, causing decreased Nox1 message and protein levels in the Nox1RNAi cell lines. Increased ROS and tumor growth in the Nox1-overexpressing DU145 cells were reversed in the presence of the Nox1RNAi. Analysis and comparison of the message levels in the overexpression and RNAi cells demonstrated that Nox1 overexpression leads to changes in message levels of a variety of proteins including c-fos-induced growth factor, interleukin-8, and Cav-1. Finally, we found that Nox1 protein overexpression is an early event in the development of prostate cancer using a National Cancer Institute prostate cancer tissue microarray (CPCTR). Tumor (86%) was significantly more likely to have Nox1 staining than benign prostate tissue (62%) ($P = 0.0001$). These studies indicate that Nox1 overexpression may function as a reversible signal for cellular proliferation with relevance for a common human tumor. ***(Am J Pathol 2007, 171:2021–2032; DOI: 10.2353/ajpath.2007.061144)***

There is a growing body of evidence that reactive oxygen plays a role in cancer. Although nontransformed cells respond to growth factors/cytokines with the regulated production of reactive oxygen species (ROS), some tumor cells produce ROS in an uncontrolled manner. A variety of human tumor-derived cell lines produced large amounts of H_2O_2 compared with nontumor cells.[1] Ras-transformed NIH 3T3 cells generated increased quantities of ROS, and antioxidants caused decreased cell growth.[2] Reactive oxygen is directly implicated in metastasis. In a study of liver metastasis by the murine colon cancer cell line COLON 26-M5 implanted in CDF1 mice, administration of recombinant human superoxide dismutase significantly increased the number of metastatic nodules whereas catalase significantly inhibited metastasis formation,[3] suggesting that H_2O_2 is the critical mediator of metastasis in this model system. Murine mammary tumor cells were significantly less adherent to laminin and fibronectin when exposed to H_2O_2, an effect that was completely blocked by catalase.[4] Catalase also partially inhibited the *in vivo* metastasis of this cell line.

Although an increase in reactive oxygen in cancer cells may be attributable to an increase in enzymes that generate reactive oxygen or a decrease in host antioxidant defenses, recent evidence suggests that NADPH oxidase 1 (Nox1) is in part responsible for increased reactive oxygen in prostate cancer cells. Nox1, a member of a family of NADPH oxidases, is an enzyme that produces superoxide, which is in turn dismuted to hydrogen peroxide. Nox1 is highly expressed in the normal colonic epithelium and to a lesser extent in vascular smooth muscle and prostate.[5] In addition, mRNA levels of Nox1, as well as Nox2 and Nox4, are up-regulated in rat ventral prostate after castration. These message levels remained elevated after testosterone replacement.[6] Several possible functions of Nox1 have been reported. Nox1 is implicated in the proliferation and hypertrophy of vascular smooth muscle cells.[7] Nox1 overexpression has been linked to colon[8] and prostate cancer[9] as well as

Supported by the National Institutes of Health/National Cancer Institute (grants CA098912 and CA96994).

Accepted for publication August 15, 2007.

Address reprint requests to John A. Petros, Department of Pathology and Laboratory Medicine, Emory University School of Medicine, 1365 Clifton Rd., Building B, Atlanta, GA 30322. E-mail: jpetros@emoryhealthcare.org.

diabetes.[10] Reactive oxygen generated by Nox1 has also been associated with increased angiogenesis.[11] In addition, it has been demonstrated that Nox1 can potentially stimulate branching morphogenesis in the nontubulogenic endothelial cell line NP 31.[12]

We have previously shown that Nox1 overexpression in human prostate cancer DU145 cells leads to increased tumorigenesis in nude mice. In addition, the tumors generated using the Nox1-overexpressing DU145 cells showed increased VEGF levels and increased microvessel density showing that Nox1 plays a role in angiogenesis.[11] A recent study demonstrated that Nox1 protein levels were increased in the prostate cancer epithelial cells compared with normal epithelial cells in 10 of 12 patients' samples examined.[9] In addition, there is a correlation between Nox1 protein levels, increased ROS production, and an increase in malignant potential. These studies suggest that Nox1 may play a role in the development of prostate cancer.

In addition to damaging DNA and oxidizing lipids, reactive oxygen can act as a mitogenic signal. In the current study, in a cell model system, we demonstrate that the increased tumor growth rate of DU145 nude mouse xenografts that overexpress Nox1 is reversible. The overexpression of Nox1 leads to reversible changes in the message levels of a variety of proteins, many of which are centrally involved in the progression and metastasis of cancer. In addition, a more comprehensive study of Nox1 protein overexpression in human prostate tissue samples demonstrates that Nox1 protein overexpression is an early event in the development of prostate cancer and that the level of Nox1 expression is independent of Gleason score, age, and racial background.

Materials and Methods

Design of RNAi

RNAi for Nox1 were designed using the algorithm available through Oligoengine (Seattle, WA). Four candidate RNAi structures were identified and the necessary forward and reverse oligonucleotides were obtained through Oligoengine and/or IDT (Coralville, IA). The oligonucleotides are as follows: 106 forward 5′-GATCCCCGGCCGACAAATACTACTACTTCAAGAGAGTAGTAGTATTTGTCGGCCTTTTTA-3′; 106 reverse 5′-TCGATAAAAAGGCCGACAAATACTACTACTCTCTTGAAGTAGTAGTATTTGTCGGCCGGG-3′; 489 forward 5′-GATCCCCCGACAGTGGAGTATGTGACTTCAAGAGAGTCACATACTCCACTGTCGTTTTTA-3′; 489 reverse 5′-TCGATAAAAACGACAGTGGAGTATGTGACTCTCTTGAAGTCACATACTCCACTGTCGGGG-3′; 819 forward 5′-GATCCCCTCCTTGCACCGGTCATTCTTTCAAGAGAAGAATGACCGGTGCAAGGATTTTTA-3′; 819 reverse 5′-TCGATAAAAATCCTTGCACCGGTCATTCTTCTCTTGAAAGAATGACCGGTGCAAGGAGGG-3′; 1267 forward 5′-GATCCCCGTGTGCAGACCACAACCTCTTCAAGAGAGAGGTTGTGGTCTGCACACTTTTTA-3′; 1267 reverse 5′-TCGATAAAAAGTGTGCAGACCACAACCTCTCTCTTGAAGAGGTTGTGGTCTGCACACGGG-3′. Oligonucleotide pairs were annealed by combining oligonucleotides in annealing buffer for a final concentration of 120 ng/μl oligonucleotides, 100 mmol/L potassium acetate, 30 mmol/L HEPES-KOH, pH 7.4, 2 mmol/L magnesium acetate. Samples were incubated for 4 minutes at 95°C, followed by incubation for 10 minutes at 70°C. Annealed samples were slowly cooled to 4°C. After phosphorylation of annealed oligonucleotides by T4 polynucleotide kinase, samples were ligated into the pSUPER vector (Oligoengine) that had been previously digested with BglII and XhoI. Clones obtained from minipreps of transformed bacteria were sequenced to verify the insertion of the RNAi into the pSUPER vector.

Transient Transfection and Assay

pSUPER Nox1 RNAi constructs were tested by transiently transfecting Nox1, NOXA1, NOXO1, and either the control vector pSUPER or one of the Nox1 RNAi constructs at a ratio of 10:1 RNAi to Nox1 into HEK 293 cells using Fugene 6 (Roche, Florence, SC) according to the manufacturer's recommended protocol. Two days after transfection, cells were detached using trypsin:ethylenediaminetetraacetic acid, pelleted, and resuspended in phosphate-buffered saline (PBS). In duplicate, 25,000 cells per transfection set were combined with 100 μl of Diogenes (National Diagnostics, Atlanta, GA), and the relative levels of superoxide were measured, in the form of chemiluminescence, using a BMG FluorStar (MTX Lab Systems, Vienna, VA).

Stable Transfection

Nox1 stable DU145 cells[11] were transfected with pSUPER or with the pSUPER Nox1 RNAi 1267 construct using Fugene 6 and following the manufacturer's protocol. After 2 days, cells were trypsin-digested and diluted 1:20 into RPMI media containing 10% fetal bovine serum, 0.5 mg/L puromycin, and 1 g/L G418. On colony formation, clones were selected using cloning disks and the cells maintained in RPMI media containing 10% fetal bovine serum, 0.5 mg/L puromycin, and 0.5 g/L G418.

Determination of Nox1 Message Levels

Total RNA was prepared from a 100-mm plate of each colony of pSUPER or Nox1 RNAi 1267 stable cells using Trizol (Invitrogen, Carlsbad, CA) according to the manufacturer's protocol. cDNA was obtained from the RNA by reverse transcription using Advantage RT for polymerase chain reaction (PCR) from Clontech (Mountain View, CA) according to the protocol. Quantitative PCR was performed to determine Nox1 levels using primers specific for human Nox1 or for human β-actin as follows: Nox1 forward: 5′-GTTTTACCGCTCCCAGCAGAA-3′; Nox1 reverse: 5′-GGATGCCATTCCAGGAGAGAG-3′; actin forward: 5′-AAAGACCTGTACTCCAACACAGTGCTGTCTGG-3′; actin reverse 5′-CGTCATACTCCTGCTTGCTGATCCACATCTGC-3′. PCR reaction was as follows: 5 μl cDNA, 0.1 μl of 10 μmol/L forward Nox1 primer or β-actin primer, 0.1 μl of 10 μmol/L reverse Nox1 or β-actin primer, 7.5 μl SYBR Green PCR Master Mix (Applied Biosystems, Foster City, CA) and 2.3 μl of water. The PCR

reaction included an initial cycle of 95°C for 10 minutes followed by 45 cycles of 95°C for 30 seconds, 56°C for 30 seconds, 72°C for 30 seconds. All results are reported as the mean starting quantities of Nox1 relative to β-actin. A 1.5% agarose gel was run after PCR, and single bands for Nox1 and for β-actin were observed. In some cases, RNA was prepared from mouse tumor tissue using the RNeasy kit (Qiagen, Valencia, CA) according to the manufacturer's protocol and message levels reported relative to 18S levels using the following primers: 18S forward: 5′-GAGTATGGTTGCAAAGCTGAAAC-3′; 18S reverse 5′-CCAGACAAATCGCTCCACCAAC-3′.

Determination of Nox1 Protein Levels

Adherent cells were harvested by first washing the plates with PBS followed by scraping cells in 1 ml of PBS containing a protease inhibitor cocktail. Cells were sonicated, on ice, 10 times for 2 seconds with microtip on power setting 4. Samples were centrifuged at 15,000 × *g*, 4°C, for 15 minutes followed by centrifugation at 200,000 × *g* for 30 minutes at 4°C. The particulate fraction was resuspended in a buffer containing 20 mmol/L Tris/HCl, pH 7.4, 6 mol/L urea, 25% glycerol, 1% Triton X-100, 0.5% deoxycholate, and 0.1% sodium dodecyl sulfate. A protein assay of the membrane suspension was performed using BCA protein assay kit (Pierce, Rockford, IL). Forty μg protein of each sample was run on a 4 to 10% bis-Tris gel for 2 hours at 125 V. Proteins were transferred to polyvinylidene difluoride membrane and washed in PBST (PBS containing 0.05% Tween) then blocked in 10% dry mild in PBST. The membrane was incubated with agitation in E39.1,[13] at a ratio of 1:500 at 4°C overnight. After three 10-minutes washes in PBST at room temperature, the membrane was incubated with a secondary anti-mouse antibody conjugated to peroxidase for 2 hours at room temperature. The membrane was washed in PBST three times for 10 minutes at room temperature. Visualization of the bands was performed using an enhanced chemiluminescence Western blotting analysis system (GE Healthcare UK, Buckinghamshire, UK) according to the manufacturer's instructions.

Dichlorofluorescein Diacetate Assays

ROS assays were performed as described previously.[9] In some cases, cells were treated with 1 mmol/L ebselen at 37°C for 15 minutes before addition of dichlorofluorescein diacetate.

Immunostaining of Stably Transfected Cells

Immunostaining was performed as described in Lim and colleagues[9] using a rabbit polyclonal antibody to Nox1.

Nude Mouse Studies

Harlan Sprague-Dawley mice, HSD.athymic nude.nu were used in this study. Mice were injected subcutaneously in the neck with either 2Du145/Nox1/pSUPER or 2DU145/Nox1/Nox1RNAi1267, 19 or 22 mice, respectively. Cells (3.6×10^6), resuspended in PBS, were injected per mouse. Mice were checked daily for tumor growth. When tumors were visually observed, they were measured length and width, and the tumor volumes calculated using the formula [length × $(\text{width})^2$]/2.[14]

Chip Experiments

Total RNA was isolated using the standard Trizol protocol and purified further with the RNeasy kit (Qiagen) according to the manufacturer's recommendations. RNA was quantified and assessed for integrity using a 2100 Bioanalyzer (Agilent Technologies, Palo Alto, CA). Expression profiles of all specimens were compared with a commercial universal reference RNA (Clontech). Probe synthesis and microarray hybridization were performed according to standard Affymetrix (Santa Clara, CA) protocols. Briefly, total RNA (5 μg per specimen) was reverse-transcribed into double-stranded cDNA, and biotin-labeled cRNA was produced by *in vitro* transcription. Labeled cRNA was fragmented and digested by DNase I before hybridization. Hybridization cocktails were prepared by combining fragmented targets, probe array controls, bovine serum albumin, and herring sperm DNA. Cocktails were applied to HG Focus oligonucleotide microarrays (Affymetrix) for 16 hours, followed by automated washing and staining on an Affymetrix workstation. After staining, microarrays were scanned and analyzed with Affymetrix Microarray Suite 5.0 software, to define probe cells, compute signal intensities in each cell, and calculate signal log2 expression ratios for each gene in tumor versus reference specimens. The HG Focus arrays produced data for 8746 genes. All hybridization experiments met the following quality control criteria: average background, <100 U; noise, <5 U; 3′:5′ ratio of control genes, <3; and RNA spikes present with appropriate signal intensities. Scaling factors and transcript presence rates varied less than 20% among samples.

Microarray Data Analysis

Affymetrix data sets were obtained from triplicate samples of Nox1-overexpressing and Nox1RNAi cells. Gene expression from each microarray, relative to a standard reference specimen, was normalized in GeneTraffic software (Iobion Informatics, La Jolla, CA) with a robust multiarray algorithm that accounted for GC content of probe sequences (GCRMA algorithm).[15] Genes were filtered to include only sequences expressed statistically above background for each replicate of either Nox1-overexpressing or Nox1RNAi cells. Differential expression in Nox1-overexpressing versus Nox1RNAi was defined as twofold over- or underexpression in each replicate. Using these criteria, 35 genes were overexpressed and 26 genes were underexpressed in the Nox1-overexpressing cell line compared with the Nox1RNAi cells. To determine whether biological processes were differentially regulated by Nox1 overexpression, the lists of overexpressed and underexpressed genes were analyzed with the GOstat program (*http://gostat.wehi.edu.au/*).[16]

Statistical Analysis of Tumor Growth Among Nude Mice

Proportions of mice developing tumors within 10 days after injection with 2Du145/Nox1/pSUPER cells (group 1) or 2Du145/Nox1/Nox1RNAi1267 cells (group 2) were compared via Fisher's exact test. Median tumor volumes were monitored throughout time among mice with discernable tumors within each group, and the median volumes were compared at day 20 after injection via the Wilcoxon rank sum test.

Immunohistochemical Staining and Analysis of Tissue Microarrays

Prostate cancer tissue microarray slides were obtained from the National Cancer Institute (NCI) Cooperative Prostate Cancer Tissue Resource (CPCTR) as NCI CPCTR TMA1 and contain 299 patient samples arrayed in quadruplicate over four slides.[17] Samples were stained for NOX1 using the Mox1 antibody (Santa Cruz Biotechnologies, Santa Cruz, CA) as previously described.[9] In brief, slides were deparaffinized in xylene and ethanol and rehydrated in water before antigen retrieval by pressure cooking in citrate buffer. After antigen blocking with rabbit antiserum, goat anti-human NOX1 was diluted 1:10 in SuperBlock (Scy Tek Laboratories, Logan, UT) and incubated 2 hours at 20°C. After washing, the slides were incubated with rabbit anti-goat secondary antibody conjugated to horseradish peroxidase (Jackson Immunoresearch, West Grove, PA) at 1:500 for 1 hour at 20°C and then washed, and the peroxidase was developed for 2 minutes after application of diaminobenzidine solution (ImmunoVision Technologies, Brisbane, CA). Specificity of the Nox1 antibody was verified by staining a control set of tissues with secondary antibody alone.

Evaluation of immunohistochemical staining was performed using methods previously described.[18,19] For each tissue core the specimen pathology (benign, high-grade prostatic intraepithelial neoplasia, or tumor), presence or absence of staining, pattern of staining (nuclear, cytoplasmic, membranous), intensity of staining (0 = no staining, 1 = weak staining less than counterstain, 2 = staining equal to counterstain, and 3 = strong staining obliterating counterstain), and notable features were assessed. Immunohistochemical staining data were correlated with patient clinical, pathological, and outcomes data collected by the NCI CPCTR.[20] For each individual patient the four representative tissue cores were analyzed for presence or absence of pathology (tumor, HGPIN, or benign prostate tissue). Where present, sample staining was evaluated for each pathological entity based on presence or absence of staining and staining intensity, with a minimum of one tissue core necessary for evaluation. When more than one tissue core demonstrated immunohistochemical staining, the staining intensity was averaged over the tissue cores. These staining patterns were correlated with the associated patient clinical, pathological, and outcomes data. Statistical analysis included the use of χ^2 analyses for categorical data and analysis of variance-based analyses for continuous variables. Regression and correlation analyses were performed using linear regression analysis. All statistical analyses were performed using the In Stat statistical software (GraphPad Software, San Diego, CA).

Results

Identification of Candidate Nox1RNAi Stable Clones

To identify which RNAi constructs were effective at decreasing Nox1 activity, constructs were first screened by transient co-transfection of Nox1, NOXA1, NOXO1, and the RNAi constructs including pSUPER, Nox1RNAi106, Nox1RNAi489, Nox1RNAi819, or Nox1RNAi1267 into HEK 293 cells. Superoxide levels were then determined as a measure of Nox1 activity. Nox1RNAi1267 was chosen for stable transfection because it inhibited Nox1-generated superoxide production approximately threefold (data not shown). Previously we demonstrated that DU145 cells stably overexpressing human Nox1 show increased tumorigenicity.[11] To demonstrate that this increased tumorigenicity was attributable to increased Nox1 in these cells, we generated DU145/Nox1 cells stably transfected with Nox1RNAi. After the generation of stable Nox1RNAi clones, the Nox1 message levels were determined using quantitative reverse transcriptase (RT)-PCR. The Nox1 message levels were significantly decreased in the Nox1RNAi1267-transfected cells (Figure 1A). Subsequently, two pSUPER-transfected and four Nox1RNAi1267 clones were analyzed for Nox1 protein levels. Figure 1B shows decreased Nox1 protein levels in a Western blot using a monoclonal antibody toward human Nox1. Human Nox1 ran at ~50 to 55 kDa, lower than the predicted 65-kDa molecular weight. Dimers and trimers of Nox1 were also observed. Analysis of Nox1 protein was repeated 10 times, loading the same amount of protein per lane. In all cases, the Nox1RNAi1267 cells showed significantly lower levels of Nox1 protein. The lower panel is a Coomassie stain of the gel to show that even amounts of protein were loaded per lane. The decrease in Nox1 protein levels in the Nox1RNAi-transfected cells correlated with decreased mRNA Nox1 levels in the same cells. In addition, immunostaining of the cells using a Nox1 polyclonal antibody demonstrated that Nox1 protein levels were decreased in the Nox1RNAi1267-transfected cells (Figure 1C).

Determination of ROS Levels

Vector- and Nox1RNAi-transfected cells were examined for changes in ROS levels. Figure 1D shows a histogram comparison of a pSUPER-transfected cell line compared with a Nox1RNAi1267-transfected cell line. The presence of Nox1RNAi1267 significantly decreased DCF fluorescence in all cell colonies when compared with pSUPER-transfected cells. Figure 1E tabulates the results of the cell lines tested. Relative

DCF fluorescence is represented as the mean value of the histogram peak. DCF fluorescent signal could be attributed to hydrogen peroxide levels. Loading the cells with exogenously added hydrogen peroxide increased the DCF fluorescence signal (Figure 1F). In addition, relative fluorescence of the DCF probe was inhibited by the presence of the antioxidant ebselen, a glutathione peroxidase mimetic. Preincubation of the cells with ebselen before DCF labeling almost completely abolished the DCF fluorescence as compared with fluorescence of the unlabeled cells. Finally, the inhibition of DCF fluorescence by ebselen was reversible. Addition of exogenously added hydrogen peroxide to the cells pretreated with ebselen after the initial DCF fluorescence measurement yielded a return of the DCF fluorescence signal.

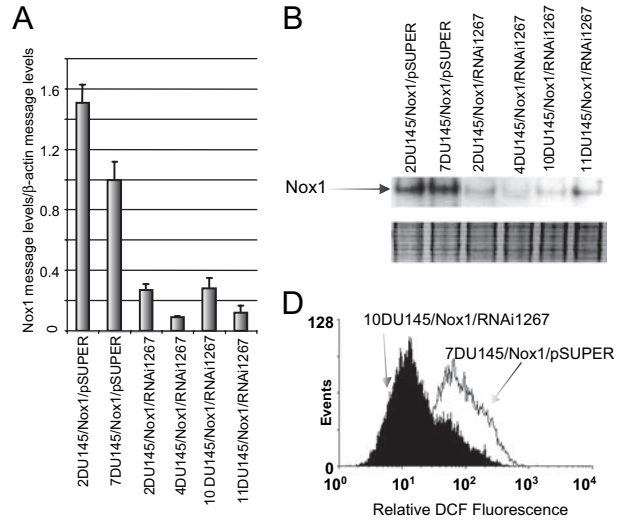

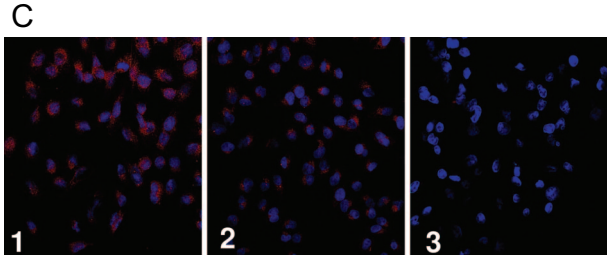

E

Cell Type	Relative DCF Fluorescence	Sample Size	p values
2DU145/Nox1/pSUPER	100.0 ± 8.0	n = 10	
7DU145/Nox1/pSUPER	148.7 ± 3.4	n = 2	
2DU145/Nox1/RNAi1267	53.1 ± 2.1	n = 6	0.002997
4DU145/Nox1/RNAi1267	55.1 ± 4.1	n = 4	0.007992
10DU145/Nox1	55.3 ± 5.7	n = 4	0.01399
11DU145/Nox1/RNAi1267	51.8 ± 5.1	n = 10	0.001706

F

Treatment of Cells	Relative Fluorescence
2DU145/Nox1/pSUPER , 0 mM ebselen, 2 μM DCFDA	100 ± 2.0
2DU145/Nox1/pSUPER , 1 mM ebselen, 2 μM DCFDA	10.0 ± 0.02
2DU145/Nox1/pSUPER , 0 mM ebselen, 2 μM DCFDA , 100 μM H_2O_2	227 ± 8.4
2DU145/Nox1/pSUPER , 1 mM ebselen, 2 μM DCFDA, 100 μM H_2O_2	171 ± 2.9
2DU145/Nox1/pSUPER , 0 mM ebselen, 0 μM DCFDA	5.5 ± 0.04

Tumor Proliferation

We have previously reported that overexpression of Nox1 in DU145 cells showed an increase in tumor growth rate, compared with DU145 cells alone, when the cells were implanted in nude mice.[11] To determine whether this increased tumorigenesis was reversible, nude mice were injected with Du145/Nox1/pSUPER or 2DU145/Nox1/Nox1RNAi1267, and tumor growth was monitored. Figure 2A demonstrates that tumor growth rate of both cell types. Mice injected with 2Du145/Nox1/pSUPER cells had measurable tumors within 10 days (16 of 16 animals). In mice injected with 2DU145/Nox1/Nox1RNAi1267 cells, only 3 of 20 mice developed tumors at 10 days ($P < 0.001$) with an average tumor volume of 0.3% that of the 2Du145/Nox1/pSUPER mice. The 2DU145/Nox1/Nox1RNAi1267 mice were associated with a highly significant delay in the first appearance of tumors relative to mice injected with 2Du145/Nox1/pSUPER cells. At day 11 the tumor volume of the 2DU145/Nox1/RNAi1267 mice was 15% of the tumor volume of the 2DU145/Nox1/pSUPER mice, at day 13 it was 37%. However, once the tumors started to appear, there was little discernable difference in their development (at least in terms of their size by day 20). Similar tumor development delays were observed with mice injected with 11DU145/Nox1/Nox1RNAi1267 cells (data not shown). *In vitro* growth curve analysis supported the *in vivo* tumor growth data, growth curves of the cell lines 2DU145/Nox1/pSUPER, 2DU145/Nox1/RNAi1267, and 11DU145/Nox1/

Figure 1. Nox1RNAi1267 constructs decrease Nox1 message, protein, and ROS levels in DU145/Nox1 stably transfected cells. DU145 cells stably overexpressing human Nox1 were stably transfected with either pSUPER vector or with the Nox1RNAi1267 construct. Cells were harvested, and RNA or protein was prepared from individual clones as described in Materials and Methods. **A:** Real-time PCR analysis of clones was performed as described in Materials and Methods. **B:** Western blot analysis of several vector-transfected and Nox1RNAi1267-transfected cell lines. Two identical gels were run of protein. The **top panel** shows the Western blot and the decreased Nox1 protein levels in the Nox1RNAi1267-transfected cells. The **bottom panel** shows the Coomassie blue-stained gel demonstrating that equal amounts of protein were loaded per lane. The experiment was repeated 10 times with similar results. **C:** Immunofluorescence staining of 2 DU145/Nox1/pSUPER (**1**) and 11 DU145/Nox1/Nox1RNAI12676 cells (**2**). Cells were stained with a rabbit polyclonal antibody to Nox1. Staining of two DU145/Nox1/pSUPER cells with secondary antibody alone is also shown (**3**). **D:** Histogram analysis of DCFDA-treated DU145/Nox1/pSUPER and DU145/Nox1/RNAi1267 cell lines as described in Materials and Methods. DU145/Nox1/RNAi1267 cells demonstrated decreased relative DCF fluorescence compared with control cells. **E:** Reactive oxygen levels are decreased in NoxRNAi1267-transfected cells. Relative DCF fluorescence of various cells lines as described in Materials and Methods. Error represents the SEM of the sample size indicated in the third column. *P* values were calculated using the Wilcoxon two sample test. The values indicated are comparisons between the indicated Nox1 RNAi cell line and the 2DU145/Nox1/pSUPER cell line. The sample size for the 7DU145/Nox1/pSUPER was too small for comparison. **F:** DCF fluorescence is a result of increased hydrogen peroxide. Relative DCF fluorescence of 2DU145/Nox1/pSUPER cell line in the presence of various factors including DCF, ebselen, and hydrogen peroxide are shown. Error is the SEM of quadruplicate samples.

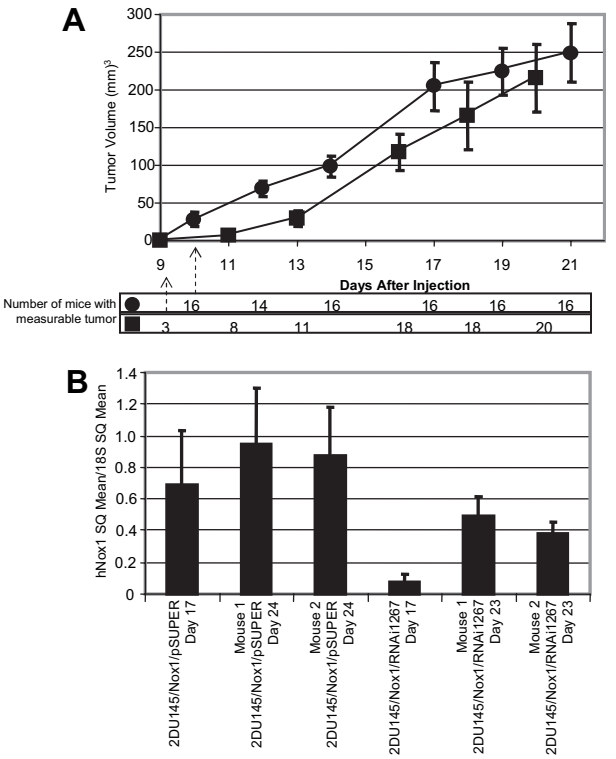

Figure 2. Delayed tumor growth in Nox1RNAi1267 xenografts. **A:** Mice were injected with 3.6×10^6 cells each per mouse (●, 16 mice, 2DU145/Nox1/pSUPER; ■, 21 mice, 2DU145/Nox1/RNAi1267). Mice were observed every other day. Tumor volume was measured as described in Materials and Methods. Error bars represent SEM of the tumor size for all mice in each set. Delay in tumor growth of 2DU145/Nox1/RNAi1267 mice compared with 2DU145/Nox1/pSUPER mice was statistically significant, $P < 0.001$ at 10 days. The number of mice in each subset that had measurable tumors at each time point measured is indicated below the graph. **B:** Total RNA was prepared from mouse tumors at day 17 and day 23, and Nox1 message levels were determined by quantitative RT-PCR as described above. Data are represented relative to 18S levels. Error bars represent the error calculated using the equation: propagation of error = $[x/y * \text{square root}((\sigma_x/x)^2 + (\sigma_y/y)^2)]$ where x = Nox1 SQ mean; y = 18S SQ mean, σ = SD.

RNAi1267 demonstrated doubling times of 1.6, 2.6, and 5.6, respectively. Two mice from each set were sacrificed at 17 days and RNA from the tumor tissue was extracted for comparison to mice sacrificed at the end of the experiment. As demonstrated by quantitative RT-PCR in Figure 2B, at day 17, the message levels for Nox1 are decreased in the tumors developed from the 2DU145/Nox1/Nox1RNAi1267-injected mice compared with mice injected with the control cells. By days 23 and 24, the Nox1 message levels are similar between the tumors from both cell types. Northern analysis of RNA showed comparable results (data not shown). These data document that the tumor growth-promoting abilities of Nox1 are reversible and that when Nox1 message levels are decreased, the tumor size is decreased, but as the Nox1 message levels increase, most likely attributable to the loss of expression of the Nox1 RNAi, so does the tumor size. Loss of the effectiveness of the RNAi construct was observable in both the tumors and the cell lines throughout successive passages (data not shown).

Gene Expression

To determine what effects overexpression of Nox1 might have on gene expression, the relative changes in message levels that can be attributed to Nox1 were determined using Affymetrix oligonucleotide microarrays containing probes for >8000 transcripts. Results from the chip analysis are shown in Tables 1 and 2. Message levels were compared with a reference standard RNA and are reported here as fold-change in comparison to the reference standard. The experiment was performed in triplicate, and only genes that showed a consistent change in all three chips are shown here. Table 1 contains a list of all genes that showed decreased message levels in the presence of the Nox1RNAi1267, indicating that the genes were up-regulated in the presence of Nox1. To the right of Table 1 are checkmarks indicating genes [Cav1, FIGF, CXCL2, interleukin (IL)-8, IL-24, and MICB] whose differential expression levels were verified by real-time PCR. Table 2 includes the genes that were increased in the presence of Nox1RNAi1267, indicating the genes that were decreased by the presence of Nox1. A number of genes associated with a variety of biological processes were demonstrated to be increased or decreased by the overexpression of Nox1. Table 3 lists the statistically overrepresented gene ontologies (international standard to annotate genes) using GOstat (*http://gostat.wehi.edu.au/*)[21] to associate the genes of interest with a biological process.

Nox1 Staining in Benign Prostate Tissue, HGPIN, and Prostate Tumors

The NCI CPCTR prostate cancer tissue microarray contained 299 patient cases. Of these samples, tumor samples were present and evaluable for 258 (86%) of the patient cases with an average of two evaluable tumor cores per patient case. In addition there were 85 evaluable patient cases with HGPIN and 140 evaluable patient cases with benign prostate tissue. Representative Nox1 staining of normal, HGPIN, and tumor (PC) is shown in Figure 3A. Nox1 staining was seen in 216 patient cases of tumor (86%), 73 cases of HGPIN (86%), and 87 cases of benign prostate tissue (62%) (Figure 3B). Tumor and HGPIN cases were significantly more likely to have Nox1 staining than benign prostate tissues ($P <= 0.0001$, χ^2 analysis), although there was no significant difference in the number of tumor and HGPIN cases with Nox1 staining. Of note, when Nox1 staining was present, HGPIN cases were significantly more likely to have stronger intensity of Nox1 staining than tumor cases (average staining 1.6/3.0 in HGPIN versus 1.4/3.0 in prostate tumors, $P < 0.0001$ by unpaired t-test). The intensity of staining was also stronger in HGPIN than in benign prostate tissues (average staining intensity 1.6/3.0 in HGPIN versus 1.3/3.0 in benign prostate tissues, $P = 0.0073$ by unpaired t-test). To examine this in more detail we studied 47 patient cases with matched benign prostate tissue, HGPIN, and prostate cancer. The average staining

Table 1. Increased Message Levels Attributed to Nox1

Gene Card ID	Descriptions	Fold change, DU145/Nox1	Fold change, Nox1RNAi	Real-time PCR
GC10P075580	Adenosine kinase (ADK), transcript variant ADK-short	3.6 ± 0.3	2.0 ± 0.6	
GC17P031415	Alternative activated macrophage-specific CC chemokine 1 (CCL18)	−3.2 ± 0.7	−5.2 ± 0.2	
GC16M065394	Amyloid beta precursor protein-binding protein 1, (APPBP1)	2.5 ± 0.2	1.2 ± 0.2	
GC10M092661	Ankyrin repeat domain 1 (ANKRD1)	2.1 ± 0.1	0.7 ± 0.6	
GC10P099322	Ankyrin repeat domain 2 (ANKRD2)	3.0 ± 0.7	0 ± 0	
GC10P045189	Arachidonate 5-lipoxygenase (ALOX5)	−2.5 ± 0.1	−3.7 ± 0.9	
GC17P003326	Aspartoacylase (aminoacylase 2, Canavan disease) (ASPA)	−3.1 ± 0.8	−5.0 ± 0.5	
GC11M027633	Brain-derived neurotrophic factor (BDNF)	2.4 ± 0.1	0.9 ± 0.3	
GC07P115719	Caveolin 1 (CAV1)	−2.0 ± 0.1	−3.2 ± 0.1	√
GC0XM015123	c-fos-induced growth factor (VEGFD, FIGF)	−2.1 ± 0.4	−3.4 ± 1.1	√
GC04M075329	Chemokine (C-X-C motif) ligand 2 (CXCL2; gro-beta)	2.1 ± 0.2	0 ± 0	√
GC17P001612	Clade F	−6.1 ± 0.2	−7.1 ± 0.5	
GC03M191506	Claudin 1 (CLDN1)	2.2 ± 0.2	0.6 ± 0.5	
GC04P075697	Epiregulin (EREG)	6.3 ± 0.2	4.6 ± 0.5	
GC15P072253	Immunoglobulin superfamily-containing leucine-rich repeat (ISLR)	−2.8 ± 0.4	−4.0 ± 0.6	
GC04M057738	Insulin-like growth factor-binding protein 7 (IGFBP7)	−7.0 ± 0.5	−9.7 ± 1.2	
GC04P075072	Interleukin 8 C-terminal variant (IL-8)	3.1 ± 0.3	0 ± 0	√
GC01P203459	Interleukin 24 (IL-24; suppression of tumorigenicity 16)	3.6 ± 0.1	0 ± 0	√
GC21P038550	Inward rectifier potassium channel (Kir1.3)	−2.8 ± 0.4	−4.7 ± 1.1	
GC04M121338	MAD2 (mitotic arrest-deficient, yeast, homolog)-like 1 (MAD2L1)	2.9 ± 0.1	1.8 ± 0.2	
GC06P031574	MHC class I polypeptide-related sequence B (MICB)	3.0 ± 0.1	1.7 ± 0.2	√
GC14M049954	Mitogen-activated protein kinase kinase kinase kinase 5 (MAP4K5)	2.8 ± 0.3	1.6 ± 0.3	
GC0XM043383	Monoamine oxidase B (MAOB)	−3.7 ± 0.3	−5.2 ± 0.6	
GC01M220721	Nuclear VCP-like (NVL)	4.0 ± 0.4	2.8 ± 0.3	
GC0XM092732	Nucleosome assembly protein 1-like 3 (NAP1L3)	−3.4 ± 0.3	−5.4 ± 1.7	
GC20P055569	Phosphoenolpyruvate carboxykinase 1 (soluble) (PCK1)	−4.7 ± 0.1	−6.8 ± 1.5	
GC12M074707	Pleckstrin homology-like domain, family A, member 1 (PHLDA1)	2.3 ± 0.2	1.1 ± 0.2	
GC07P116187	Potential tumor suppressor (ST7)	5.1 ± 0.5	3.6 ± 0.7	
GC16M011282	Protamine 1 (PRM1)	−5.1 ± 0.4	−6.8 ± 0.1	
GC08P080685	Superior cervical ganglia, neural-specific 10 (SCGN10)	−4.4 ± 0.4	−−6.8 ± 0.3	
GC0XM047187	Synapsin I (SYN1)	−3.2 ± 0.5	−5.2 ± 0.9	
GC02M218492	Tensin (TNS1)	−5.5 ± 0.3	−7.8 ± 0.3	
GC20P054637	Transcription factor AP-2 alpha (TFAP2A)	2.6 ± 0.1	1.6 ± −0.1	
GC01P117314	Transcription termination factor, RNA polymerase II (TTF2)	2.5 ± 0.2	0.4 ± 0.7	
GC02P234364	UDP glycosyltransferase 1 family, polypeptide A3 (UGT1A3)	−2.1 ± 0	−3.9 ± 1.2	

Affymetric DNA array analysis was performed on 2 DU145/Nox1/pSUPER and 11 DU145/Nox1/Nox1RNAI12676 cells as described in Materials and Methods. Fold changes represent the average and standard deviation of three samples. Only messages that showed consistently increased or decreased message levels in all three samples were analyzed using *http://gostat.wehi.edu.au/*. The check marks to the right of the table indicate the changes that have been confirmed through real-time PCR. Gene Card ID numbers are listed as described at *http://genecards.org/index.html*.

intensity was 0.90 ± 0.91, 1.37 ± 0.76, and 1.31 ± 0.61 in benign, HGPIN, and tumor tissue, respectively. In these specimens the significant increase in staining intensity in HGPIN and cancer was statistically different from the staining intensity in benign prostate tissues ($P = 0.0078$, Friedman test nonparametric repeated measures analysis of variance), confirming the central findings in tissue microarray.

Nox1 Tumor Staining and Pathological and Outcomes Parameters

Nox1 tumor staining was evaluated with respect to clinical, pathological, and outcomes parameters (Table 4). In 248 patient cases race was known, with 30 African-Americans and 217 European-Americans. Only one Asian-American was identified and was demonstrated to exhibit Nox1-positive staining. No significant association was noted between Nox1 staining and African-American or European-American ancestry. The overall average age for the patient cases was 65.1 years, and no significant difference was noted between Nox1-positive and -negative tumors and patient age. All 258 patient cases in which tumors were evaluated had undergone radical prostatectomy as the initial definitive treatment for their prostate cancer. When pathological parameters for the radical prostatectomy specimens were evaluated with respect to prostate tumor TMA Nox1 staining, no significant differences were noted between the presence or absence of Nox1 staining and high Gleason score (Gleason score 5 to 6 versus 7 to 9), pathological tumor stage, or pathological lymph node status. Prostate-specific antigen (PSA) nadir status and PSA recurrence status was known in 162 and 103 patient cases, respectively. In cases in which PSA recurrence was calculated, the average follow-up time was 4.96 years. Nox1 staining was not significantly correlated with either failure to nadir after surgery or subsequent PSA recurrence status. Vital sta-

Table 2. Decreased Message Levels Attributed to Nox1

Gene Card ID	Descriptions	Fold change, DU145/Nox	Fold change, Nox1RNAi
GC19M053825	Albumin D-box binding protein (DBP)	−3.0 ± 0.7	−1.4 ± 0.2
GC19P041051	Amyloid precursor-like protein 1 (APLP1)	−4.9 ± 0.4	−3.5 ± 0.1
GC17P007494	ATPase, Na^+K^+ transporting, beta 2 polypeptide (ATP1B2)	−3.9 ± 1.2	−2.6 ± 0.3
GC19P054149	BCL2-associated X protein (BAX)	−2.4 ± 0.9	−0.4 ± 0.6
GC11M066088	Cathepsin F (CTSF)	−4.6 ± 0.6	−2.9 ± 0.2
GC08P027224	Cell adhesion kinase beta (CAKbeta, PTK2B)	−3.3 ± 0.6	−1.4 ± 0.3
GC11P065536	Cystatin EM (CST6)	−3.1 ± 1.6	−1.7 ± 0.4
GC01P046976	Cytochrome P450 (IV subfamily) BI (CYP4B1)	−5.3 ± 1.7	−3.4 ± 0.2
GC13M070910	Dachshund (Drosophila) homolog (DACH1)	−2.6 ± 0.9	−1.6 ± 0.1
GC10M044791	Decidual protein induced by progesterone (DEPP)	−4.9 ± 0.5	−3.3 ± 0.3
GC13M035243	Double cortin and CaM kinase-like 1 (DCAMKL1)	−3.8 ± 0.4	−2.1 ± 0.2
GC06M052723	Glutathione *S*-transferase A2 (GSTA2)	−6.0 ± 0.2	−4.5 ± 0.4
GC07M045725	Insulin-like growth factor binding protein 3 (IGFBP3)	−3.2 ± 0.3	−1.9 ± 0.2
GC17P035854	Insulin-like growth factor-binding protein 4 (IGFBP4)	−4.7 ± 0.5	−3.5 ± 0.2
GC11M000309	Interferon-induced transmembrane protein 3 (1-8U, IFITM3)	−7.6 ± 0.7	−4.5 ± 0.1
GC10M069226	J domain-containing protein 1 (JDP1)	2.2 ± 0.2	3.4 ± 0.2
GC15P028915	Kruppel-like factor 13 (KLF13)	−3.3 ± 0.8	−1.2 ± 1.1
GC19M047597	Lipase, hormone-sensitive (LIPE)	−4.1 ± 0.5	−2.5 ± 0.7
GC06M136705	Microtubule-associated protein 7 (MAP7)	−2.5 ± 1.2	0.2 ± 0.2
GC04M175786	NAD^+-dependent 15-hydroxyprostaglandin dehydrogenase (HPDG)	−4.3 ± 0.1	−0.6 ± 0.6
GC11P124114	Neurogranin (protein kinase C substrate, RC3) (NRGN)	−5.8 ± 0.8	−4.8 ± 0.3
GC01M150330	S100 calcium-binding protein A4 (S100A4)	−3.0 ± 0.4	−1.1 ± 0.1
GC20M043314	Secretory leukocyte protease inhibitor (anti-leukoproteinase) (SLPI)	−2.9 ± 0.1	−1.8 ± 0.1
GC14M022895	Signal transduction protein (SH3 containing) (EFS2)	−4.0 ± 0.7	−2.0 ± 0.5
GC01P175994	Sterol *O*-acyltransferase (SOAT1)	−5.3 ± 0.4	−3.3 ± 0.3
GC01P142927	Up-regulated by 1,25-dihydroxyvitamin D-3 (VDUP1)	−4.7 ± 0.2	−3.3 ± 0.1

Affymetric DNA array analysis was performed on 2 DU145/Nox1/pSUPER and 11 DU145/Nox1/Nox1RNAI12676 cells as described in Materials and Methods. Fold changes represent the average and standard deviation of three samples. Only messages that showed consistently increased or decreased message levels in all three samples were analyzed using *http://gostat.wehi.edu.au/*. Gene Card ID numbers are listed as described at *http://genecards.org/index.html*.

tus was available on all 258 patient cases and did not correlate with Nox1 staining.

An analysis of the 206 patient cases, with positive Nox1 tumor staining, for relationships between Nox1 staining intensity and clinical, pathological, and outcomes parameters was also performed. No significant correlations were noted between patient race and Nox1 intensity of staining (data not shown). To evaluate further the correlation between patient age and Gleason score, we examined the staining intensity with respect to these continuous variables by linear regression. Linear regression analysis failed to identify any significant correlation with patient age (data not shown). Patient case outcomes were also analyzed with respect to Nox1 staining intensity

Table 3. Overrepresented Gene Ontologies

Gene ontology	Count	Total genes	*P* value
Angiogenesis	3	53	0.000116
Development	12	2127	0.00026
Organogenesis	8	1026	0.000409
Morphogenesis	9	1307	0.000426
Cell differentiation	5	384	0.000585
Cytokine activity	4	244	0.000924
Receptor binding	6	731	0.00179
Growth factor activity	3	212	0.00636
Neurogenesis	4	448	0.00816
Cell communication	16	4919	0.0112
Cell proliferation	4	526	0.0141
Cell cycle	5	853	0.0173

The Affymetric's ID numbers were checked against all genes in the GO (gene ontology) associations database. GO statistics of the genes from the microarray that were increased or decreased by the overexpression of Nox1 are listed. GOstat (*http://gostat.wehi.edu.au/*) was used to find statistically overrepresented gene ontologies. The genes represented were determined with the criteria of *P* value <0.01.

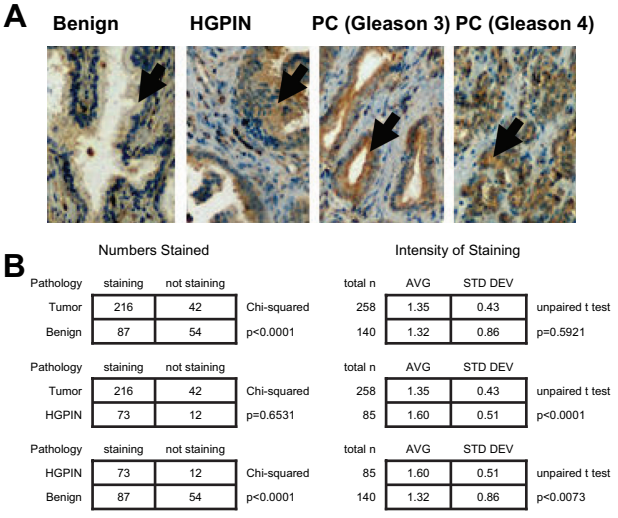

Figure 3. Nox1 overexpression in HGPIN and cancer in human prostate tissue. **A:** Human prostate tissue was analyzed for Nox1 protein expression using immunohistochemical analysis as described in Materials and Methods. **Arrows** point to the prostate epithelial cells. Representative pictures of the normal prostate epithelial, HGPIN, and prostate cancer (Gleason 3 and Gleason 4) are shown. **B:** Overall NOX1 staining in benign prostate tissue, HGPIN, and prostate tumors. Analysis was performed as described in Materials and Methods. *P* values are a result of either χ^2 or unpaired *t*-test analysis.

Table 4. NOX1 Tumor Staining with Respect to Clinical, Pathological, and Outcome Parameters

Tumor staining	No	Yes	
Race			$P = 0.5933$
African-American	6	24	
Caucasian	35	182	
Age			Unpaired *t*-test
average	65.6	65	P = 0.5390
SD	6.9	6	
n	42	216	
Gleason sum score			$P = 0.1578$
5 to 6	9	70	
7 to 9	33	146	
pT stage			$P = 0.4087$
pT2	23	133	
pT3 and pT4	19	83	
pN stage			$P = 0.4528$
pN0	35	195	
pN1	2	6	
pNX	5	15	
PSA nadir status			$P = 0.6378$
No nadir	9	50	
Nadir	13	90	
Unknown	20	76	
PSA recurrence status			$P = 0.9002$
Yes	5	33	
No	8	57	
Unknown	20	76	
Vital status			$P = 0.3728$
Alive	30	168	
Deceased	12	48	

Tissue staining was analyzed with respect to clinical,pathological, and outcome parameters as described in the Materials and Methods. Unless otherwise indicated, *P* values are a result of χ^2 analysis.

but failed to identify any significant correlations between the intensity of Nox1 staining in either PSA nadir status, PSA recurrence status, or vital status (data not shown).

Discussion

We have observed increased Nox1 protein expression by immunohistochemical staining in prostate tumors when compared with benign prostate tissues. This up-regulation of Nox1 expression appears to be an early event in prostatic neoplasia because Nox1 expression is also up-regulated in HGPIN, a pathological precursor lesion for prostate cancer. The increase in Nox1 expression is seen not only in individual prostate tissues, but also in a progression series of benign, precancer, and cancer specimens from the same patients. These results suggest a role for Nox1 in early prostatic neoplasia.

The lack of correlation between Nox1 expression and clinical or pathological parameters of prostate cancers confirm the early role Nox1 plays in prostatic neoplasia and downplays its role in the development of aggressive prostate cancers. The lack of correlation between Nox1 expression and aggressive prostate cancer is also supported by the lack of correlations between Nox1 expression and patient outcome.

Aging is correlated with increasing oxidative damage and associated increased cancer risk. We found no correlation between Nox1 expression and age. If such a correlation was seen it could imply that the correlation between Nox1 and prostate cancer reflects the age of the prostate cancer population. This is not the case and helps to associate the effects of Nox1 with prostate cancer regardless of age.

Because previous work by our laboratory demonstrated an increase in Nox1 protein levels in prostate cancer epithelial cells compared with normal epithelium,[9] we sought to understand the molecular changes induced by Nox1. This was accomplished by both forced overexpression of Nox1 in cancer cell lines and the knockdown of Nox1 expression by RNAi. We found both gene expression and cell biological consequences of Nox1 overexpression that position Nox1 as a key mediator of the malignant phenotype. Furthermore, the growth-enhancing effects of Nox1 were confirmed *in vivo* in nude mouse xenograft experiments. A more rigorous analysis of Nox1 protein levels in human prostate tissue demonstrated that Nox1 overexpression is a consistent feature of transformed prostatic epithelium, remains constant across all clinical subgroups of prostate cancer patients, and remains present even in high-grade and advanced stage disease. This concordance of results in clinical and laboratory models lends credence to the central hypothesis that Nox1 overexpression is a consistent finding and functional mediator of prostatic epithelial transformation.

Immunohistochemical analysis of clinical prostate cancer specimens has documented that the superoxide anion-generating Nox1 enzyme is overexpressed in a cancer-specific manner in more than 80% of all tumors. Previous laboratory analyses support the hypothesis that the overexpression of Nox1 promotes tumorigenesis and angiogenesis and is not simply an associated or secondary phenomenon. The work presented in this report demonstrates that this effect is primarily attributable to dynamic signaling effects rather than fixed alterations such as DNA mutations. *In vivo* human tumor xenograft experiments reveal that tumor growth rates are high when Nox1 expression is high and low when Nox1 expression is low. We have performed gene expression analysis on pairs of cell lines that differ only in the level of Nox1 expression. Several key regulators of the malignant phenotype are regulated by Nox1 expression in a coordinated way to enhance tumor growth. These include the induction of c-fos-induced growth factor (FIGF/VEGF-D) and IL-8, both of which have been previously shown to play important roles in prostate cancer tumor growth and/or angiogenesis.

The increase in tumor growth caused by the overexpression of Nox1 may be in part explained by the effect of Nox1, and by inference ROS, on the message levels of a variety of proteins that are involved in processes relevant to cancer such as apoptosis, inflammation and immune function, and growth and angiogenesis as shown in Tables 1 and 2. The following discussion highlights changes observed in several messages involved in apoptosis, growth and angiogenesis, and inflammation and immune function. The genes dis-

cussed have all been verified by real-time PCR to increase in Nox1-overexpressing cells.

The message levels for a number of proteins involved in signal transduction, growth, and angiogenesis are regulated by the presence of Nox1. In particular, the message levels for c-*fos*-induced growth factor (FIGF/VEGF-D) and IL-8 are increased by Nox1. There is strong evidence in the literature to indicate that these proteins play an important role in growth and/or angiogenesis in prostate cancer. FIGF/VEGF-D might play a critical role in tumor growth and angiogenesis. FIGF/VEGF-D, which is under the control of the nuclear oncogene c-fos, induces angiogenesis and lymphangiogenesis *in vivo* and *in vitro*.[21] High expression of FIGF/VEGF-D is associated with advanced stage metastatic prostate cancer.[22] FIGF/VEGF-D is significantly up-regulated in primary tumor specimens compared with tissue isolated from benign prostatic hyperplasia.[23] IL-8 has been implicated in the growth and metastasis of cancer. Ras-induced IL-8 expression was required for the initiation of tumor-associated inflammation and neovascularization in a tumor xenograft model.[24] Interestingly, the Ras oncogene up-regulates the expression of Nox1, which is required for Ras-mediated transformation.[25] IL-8 is associated with androgen-independent prostate cancer growth and advanced stage prostate cancer.[26,27] These data implicate elevation of Nox1 in events leading to the development of androgen-dependent growth and advanced stage prostate cancer.

Dysregulation of apoptosis is one event leading to the uncontrolled growth of cancer cells. The message levels of several proteins that regulate apoptosis are regulated by Nox1, including IL-24 (mda7/IL-24) and caveolin-1 (Cav-1). The role of caveolin-1 as proapoptotic or anti-apoptotic is dependent on cell type. In prostate cancer cells, Cav-1 has an anti-apoptotic effect. Overexpression of Cav-1 in a prostate cancer cell line (LNCaP) or up-regulation of Cav-1 in androgen-insensitive prostate cancer cells renders these cells resistant to apoptosis.[28,29] Cav-1 is consistently up-regulated in a variety of cancers, including bladder, esophagus, thyroid (papillary subtype), and prostate, whereas it is consistently down-regulated in others, including ovarian, lung, and breast cancers.[30] Increased Cav-1 has been linked to metastasis in prostate cancer. Cav-1 expression showed a positive correlation with Gleason score and lymph node involvement.[31,32] Antisense-mediated down-regulation of Cav-1 in prostate cancer cells reduced their metastatic phenotype.[28,33] Our data shows that Nox1 is involved in the increased level of Cav-1 in prostate cancer cells.

A characteristic of mda7/IL-24 is its capacity to induce apoptosis in cancer cells. Increased levels of mda7/IL-24 in a variety of cancer cells, such as pancreatic cancer, prostate cancer, and ovarian cancer, kill the cancer cells.[34–36] In clinical samples of lung adenocarcinoma, whereas there was no significant correlation between mda7/IL-24 staining and pathological stage, a positive mda7/IL-24 staining was a significant factor to predict a favorable prognosis.[37] In this study, Nox1 increases the level of mda7/IL-24. Although increased message levels of a proapoptotic protein was surprising it is possible that this represents a compensatory response to overall growth stimulation.

A role for Nox1 in host defense has been proposed. Based on its distribution in colon tissue it may be involved in the pathogenesis of inflammatory bowel disease.[38] The role of inflammation in carcinogenesis, tumor promotion, invasion, and metastasis is increasingly understood to be important. One example of a specific type of cancer linked to inflammation is gastric cancer. There is a strong positive correlation between *Helicobacter pylori* infection and stomach cancer.[39,40] Interestingly, live *H. pylori* significantly increased superoxide production in guinea pig gastric mucosal cells[41] via stimulation of Nox1 transcription by *H. pylori* lipopolysaccharide.[42]

Chemokines are members of a large superfamily of structurally and functionally related inflammatory cytokines that stimulate the chemotactic migration of distinct sets of cells, including neutrophils, monocytes, lymphocytes, and fibroblasts. Chemokines are involved in many events necessary for tumor development including angiogenesis, invasion of the extracellular matrix, and metastasis.[43] A number of chemokines are regulated by Nox1. For example, message levels for CXCL2 (Gro β) were elevated by Nox1. CXCL2 has been linked to angiogenesis in Lewis Lung carcinoma[44] as well as melanoma growth and migration.[45]

MICA and MICB are homologs of MHC class I, recently recognized as tumor-associated antigens that can be recognized, in an apparently unconditional manner, by a subset of tumor-infiltrating T cells. MICA/B are detected in several types of cancer, including lung, ovary, breast, colon, and prostate, and it has been hypothesized that MICA/B functions as a component of an innate immune surveillance of tumors.[46] In agreement with the increased MICB levels detected in prostate cancer, our data show that Nox1 increases the message levels of MICB. Oxidative stress increases MICB gene expression in human colon cancer cells, and H_2O_2 induces an increase in MICB gene expression in CaCo2 cells. This data are in agreement with increased MICB in our cells that demonstrate an increase in H_2O_2 production.

The data described here demonstrate for the first time that up-regulation of Nox1 expression is an early event in prostate carcinogenesis. In addition, the data demonstrate that the increase in tumor proliferation that results from increased Nox1 expression in DU145 prostate cancer cells is reversible on removal of Nox1. Specific intermediaries of Nox1 signaling are outlined including c-fos-induced growth factor (FIGF/VEGF-D), IL-8, Cav-1, mda7/IL-24, CXCL2 (Gro β), and MICB, all of which have been previously shown to play important roles in malignant transformation.

Acknowledgments

We thank Robert H. Lyles for his assistance in determining the statistical analysis of tumor growth among nude

mice; and Drs. Fray Marshall, Tristram Parslow, and Jonathan Simons for departmental support.

References

1. Burdon RH: Control of cell proliferation by reactive oxygen species. Biochem Soc Trans 1996, 24:1028–1032
2. Irani K, Xia Y, Zweier J, Sollott S, Der C, Rearon E, Sundaresan M, Finkel T, Goldschmidt-Clermont P: Mitogenic signaling mediated by oxidants in Ras-transformed fibroblasts. Science 1997, 275:1649–1652
3. Nonaka Y, Iwagaki H, Kimura T, Fuchimoto S, Orita K: Effect of reactive oxygen intermediates on the in vitro invasive capacity of tumor cells and liver metastasis in mice. Int J Cancer 1993, 54:983–986
4. Kundu N, Zhang S, Fulton AM: Sublethal oxidative stress inhibits tumor cell adhesion and enhances experimental metastasis of murine mammary carcinoma. Clin Exp Metastasis 1995, 13:16–22
5. Suh YA, Arnold RS, Lassegue B, Shi J, Xu X, Sorescu D, Chung AB, Griendling KK, Lambeth JD: Cell transformation by the superoxide-generating oxidase Mox1. Nature 1999, 401:79–82
6. Tam NN, Gao Y, Leung YK, Ho SM: Androgenic regulation of oxidative stress in the rat prostate: involvement of NAD(P)H oxidases and antioxidant defense machinery during prostatic involution and regrowth. Am J Pathol 2003, 163:2513–2522
7. Griendling KK, Sorescu D, Ushio-Fukai M: NAD(P)H oxidase: role in cardiovascular biology and disease. Circ Res 2000, 86:494–501
8. Fukuyama M, Rokutan K, Sano T, Miyake H, Shimada M, Tashiro S: Overexpression of a novel superoxide-producing enzyme. NADPH oxidase 1, in adenoma and well differentiated adenocarcinoma of the human colon. Cancer Lett 2005, 221:97–104
9. Lim SD, Sun CQ, Lambeth JD, Marshall F, Amin M, Chung L, Petros JA, Arnold RS: Increased Nox1 and hydrogen peroxide in prostate cancer. Prostate 2005, 62:200–207
10. Mahadev K, Motoshima H, Wu X, Ruddy JM, Arnold RS, Cheng G, Lambeth JD, Goldstein BJ: The NAD(P)H oxidase homolog Nox4 modulates insulin-stimulated generation of H2O2 and plays an integral role in insulin signal transduction. Mol Cell Biol 2004, 24:1844–1854
11. Arbiser JL, Petros J, Klafter R, Govindajaran B, McLaughlin ER, Brown LF, Cohen C, Moses M, Kilroy S, Arnold RS, Lambeth JD: Reactive oxygen generated by Nox1 triggers the angiogenic switch. Proc Nat Acad Sci USA 2001, 99:715–720
12. Kobayashi S, Nojima Y, Shibuya M, Maru Y: Nox1 regulates apoptosis and potentially stimulates branching morphogenesis in sinusoidal endothelial cells. Exp Cell Res 2004, 300:455–462
13. Kawahara T, Ritsick D, Cheng G, Lambeth JD: Point mutations in the proline-rich region of p22phox are dominant inhibitors of Nox1- and Nox2-dependent reactive oxygen generation. J Biol Chem 2005, 280:31859–31869
14. Hammond-McKibben D, Lake P, Zhang J, Tart-Risher N, Hugo R, Weetall M: A high capacity quantitative mouse model of drug-mediated immunosuppression based on rejection of an allogeneic subcutaneous tumor. J Pharmacol Exp Ther 2001, 297:1144–1151
15. Bolstad BM, Irizarry RA, Astrand M, Speed TP: A comparison of normalization methods for high density oligonucleotide array data based on variance and bias. Bioinformatics 2003, 19:185–193
16. Beissbarth T, Speed TP: GOstat: find statistically overrepresented gene ontologies within a group of genes. Bioinformatics 2004, 20:1464–1465
17. Melamed J, Datta MW, Becich MJ, Orenstein JM, Dhir R, Silver S, Fidelia-Lambert M, Kadjacsy-Balla A, Macias V, Patel A, Walden PD, Bosland MC, Berman JJ: The cooperative prostate cancer tissue resource: a specimen and data resource for cancer researchers. Clin Cancer Res 2004, 10:4614–4621
18. Datta MW, Renshaw AA, Dutta A, Hoffman MA Loughlin KR: Evaluation of cyclin expression in testicular germ cell tumors: cyclin E correlates with tumor type, advanced clinical stage, and pulmonary metastasis. Mod Pathol 2000, 13:667–672
19. Osipov V, Keating JT, Faul PN, Loda M, Datta MW: Expression of p27 and VHL in renal tumors. Appl Immunohistochem Mol Morphol 2002, 10:344–350
20. Patel AA, Kajdacsy-Balla A, Berman JJ, Bosland M, Datta MW, Dhir R, Gilbertson J, Melamed J, Orenstein J, Tai KF, Becich MJ: The development of common data elements for a multi-institute prostate cancer tissue bank: the Cooperative Prostate Cancer Tissue Resource (CPCTR) experience. BMC Cancer 2005, 5:108
21. Marconcini L, Marchio S, Morbidelli L, Cartocci E, Albini A, Ziche M, Bussolino F, Oliviero S: c-fos-induced growth factor/vascular endothelial growth factor D induces angiogenesis in vivo and in vitro. Proc Natl Acad Sci USA 1999, 96:9671–9676
22. Kaushalk V, Mukunyadzi P, Dennis RA, Siegel ER, Johnson DE, Kohli M: Stage-specific characterization of the vascular endothelial growth factor axis in prostate cancer: expression of lymphangiogenic markers is associated with advanced-stage disease. Clin Cancer Res 2005, 11:584–593
23. Stearns ME, Wang M, Hu Y, Kim G, Garcia FU: Expression of a flt-4 (VEGFR3) splicing variant in primary human prostate tumors. VEGF D and flt-4t(Delta773-1081) overexpression is diagnostic for sentinel lymph node metastasis. Lab Invest 2004, 84:785–795
24. Sparmann A, Bar-Sagi D: Ras-induced interleukin-8 expression plays a critical role in tumor growth and angiogenesis. Cancer Cell 2004, 6:447–458
25. Mitsushita J, Lambeth JD, Kamata T: The superoxide-generating oxidase Nox1 is functionally required for Ras oncogene transformation. Cancer Res 2004, 64:3580–3585
26. Lee LF, Louie MC, Desai SJ, Yang J, Chen HW, Evans CP, Kung HJ: Interleukin-8 confers androgen-independent growth and migration of LNCaP: differential effects of tyrosine kinases Src and FAK. Oncogene 2004, 23:2197–2205
27. Uehara H, Troncoso P, Johnston D, Bucana CD, Dinney C, Dong Z, Fidler IJ, Pettaway CA: Expression of interleukin-8 gene in radical prostatectomy specimens is associated with advanced pathologic stage. Prostate 2005, 64:40–49
28. Li L, Yang G, Ebara S, Satoh T, Nasu Y, Timme TL, Ren C, Wang J, Tahir SA, Thompson TC: Caveolin-1 mediates testosterone-stimulated survival/clonal growth and promotes metastatic activities in prostate cancer cells. Cancer Res 2001, 61:4386–4392
29. Li L, Ren CH, Tahir SA, Ren C, Thompson TC: Caveolin-1 maintains activated Akt in prostate cancer cells through scaffolding domain binding site interactions with and inhibition of serine/threonine protein phosphatases PP1 and PP2A. Mol Cell Biol 2003, 23:9389–9404
30. Williams TM, Lisanti MP: Caveolin-1 in oncogenic transformation, cancer, and metastasis. Am J Physiol 2005, 8:C494–C506
31. Satoh T, Yang G, Egawa S, Addai J, Frolov A, Kuwao S, Timme TL, Baba S, Thompson TC: Caveolin-1 expression is a predictor of recurrence-free survival in pT2N0 prostate carcinoma diagnosed in Japanese patients. Cancer 2003, 97:1225–1233
32. Yang G, Truong LD, Wheeler TM, Thompson TC: Caveolin-1 expression in clinically confined human prostate cancer: a novel prognostic marker. Cancer Res 1999, 59:5719–5723
33. Nasu Y, Timme TL, Yang G, Bangma CH, Li L, Ren C, Park SH, DeLeon M, Wang J, Thompson TC: Suppression of caveolin expression induces androgen sensitivity in metastatic androgen-insensitive mouse prostate cancer cells. Nat Med 1998, 4:1062–1064
34. Chada S, Bocangel D, Ramesh R, Grimm EA, Mumm JB, Mhashilkar AM, Zheng M: mda-7/IL24 kills pancreatic cancer cells by inhibition of the Wnt/PI3K signaling pathways: identification of IL-20 receptor-mediated bystander activity against pancreatic cancer. Mol Ther 2005, 11:724–733
35. Lebedeva IV, Sarkar D, Su ZZ, Kitada S, Dent P, Stein CA, Reed JC, Fisher PB: Bcl-2 and Bcl-x(L) differentially protect human prostate cancer cells from induction of apoptosis by melanoma differentiation associated gene-7, mda-7/IL-24. Oncogene 2003, 22:8758–8773
36. Gopalan B, Litvak A, Sharma S, Mhashilkar AM, Chada S, Ramesh R: Activation of the Fas-FasL signaling pathway by MDA-7/IL-24 kills human ovarian cancer cells. Cancer Res 2005, 65:3017–3024
37. Ishikawa S, Nakagawa T, Miyahara R, Kawano Y, Takenaka K, Yanagihara K, Otake Y, Katakura H, Wada H, Tanaka F: Expression of MDA-7/IL-24 and its clinical significance in resected non-small cell lung cancer. Clin Cancer Res 2005, 11:1198–1202
38. Szanto I, Rubbia-Brandt L, Kiss P, Steger K, Banfi B, Kovari E, Herrmann F, Hadengue A, Krause KH: Expression of NOX1, a super-

oxide-generating NADPH oxidase, in colon cancer and inflammatory bowel disease. J Pathol 2005, 207:164–176
39. Eslick GD, Lim LL, Byles JE, Xia HH, Talley NJ: Association of Helicobacter pylori infection with gastric carcinoma: a meta-analysis. Am J Gastroenterol 1999, 94:2373–2379
40. Blaser MJ, Perez-Perez GI, Kleanthous H, Cover TL, Peek RM, Chyou PH, Stemmermann GN, Nomura A: Infection with Helicobacter pylori strains possessing cagA is associated with an increased risk of developing adenocarcinoma of the stomach. Cancer Res 1995, 55:2111–2115
41. Teshima S, Rokutan K, Nikawa T, Kishi K: Guinea pig gastric mucosal cells produce abundant superoxide anion through an NADPH oxidase-like system. Gastroenterology 1998, 115:1186–1196
42. Kawahara T, Kohjima M, Kuwano Y, Mino H, Teshima-Kondo S, Takeya R, Tsunawaki S, Wada A, Sumimoto H, Rokutan K: Helicobacter pylori lipopolysaccharide activates Rac1 and transcription of NADPH oxidase Nox1 and its organizer NOXO1 in guinea pig gastric mucosal cells. Am J Physiol 2005, 288:C450–C457
43. Vicari AP, Caux C: Chemokines in cancer. Cytokine Growth Factor Rev 2002, 13:143–154
44. Saijo Y, Tanaka M, Miki M, Usui K, Suzuki T, Maemondo M, Hong X, Tazawa R, Kikuchi T, Matsushima K, Nukiwa T: Proinflammatory cytokine IL-1 beta promotes tumor growth of Lewis lung carcinoma by induction of angiogenic factors: in vivo analysis of tumor-stromal interaction. J Immunol 2002, 169:469–475
45. Gallagher PG, Bao Y, Prorock A, Zigrino P, Nischt R, Politi V, Mauch C, Dragulev B, Fox JW: Gene expression profiling reveals cross-talk between melanoma and fibroblasts: implications for host-tumor interactions in metastasis. Cancer Res 2005, 65:4134–4146
46. Groh V, Rhinehart R, Secrist H, Bauer S, Grabstein KH, Spies T: Broad tumor-associated expression and recognition by tumor-derived gamma delta T cells of MICA and MICB. Proc Natl Acad Sci USA 1999, 96:6879–6884